

FEDSM-ICNMM2010-' \$+))

AN EXPERIMENTAL STUDY OF BOUNDARY-LAYER TRANSITION INDUCED VIBRATIONS ON A HYDROFOIL

Antoine Ducoin*

Postdoctoral fellow

Department of Naval Architecture & Marine Engineering
University of Michigan
2600 Draper Dr,
Ann Arbor, Michigan 48109
Email: aducoin@umich.edu

Jacques André Astolfi

Marie-Laure Gobert

Institut de Recherche de l'Ecole Navale
(IRENav) EA 3634
BCRM Brest, CC 600
29240 Brest cedex 9, France
Email: jacques-andre.astolfi@ecole-navale.fr

ABSTRACT

In this paper, we investigate through an experimental approach the laminar to turbulent transition in the boundary-layer flow along a hydrofoil at a Reynolds number of 7.5×10^5 , together with the vibrations of the hydrofoil induced by the transition. The latter is caused by a Laminar Separation Bubble (LSB) resulting from a laminar separation of the boundary-layer. The experiments, conducted in the hydrodynamic tunnel of the Research Institute of the French Naval Academy, are based on wall pressure and flow velocity measurements along a rigid hydrofoil, which enable a characterization of the Laminar Separation Bubble and the identification of a vortex shedding at a given frequency. Vibrations measurements are then carried out on a flexible hydrofoil in the same operating conditions. The results indicate that the boundary-layer transition induces important vibrations, whose characteristics in terms of frequency and amplitude depend on the vortex shedding frequency, and can be coupled with natural frequencies.

INTRODUCTION

The hydrodynamic loading prediction on control surfaces requires a good knowledge of the boundary-layer flow regime around the body. For instance, the control surfaces of Autonomous Underwater Vehicles (AUV) can operate at

transitional regimes due to their relatively small scales. The apparition of the transition in the boundary-layer flow may affect their hydrodynamic performances and be responsible for the generation of vibrations. Typically, the transition on lifting bodies occurs at low to moderate Reynolds numbers and is triggered by a separated flow region due to an adverse pressure gradient. The development of the turbulent flow, which causes a momentum transfer in the wall normal direction, allows the flow to reattach. This phenomenon can also appear at higher Reynolds numbers on laminar sections, designed in the marine industry for the propeller blades, which promote a laminar boundary-layer flow along their chords. However, because of the large Reynolds number, a very strong and located vorticity region may occur and affect the pressure distribution.

Many studies have been dedicated to the issue of laminar separation, in particular for aerodynamic applications on flat plates and lifting bodies. The Laminar Separation Bubble (LSB) on hydrofoils at moderate Reynolds numbers has been given a special interest, from the pioneer experimental works of Gaster (1969) [1] or Tani (1964) [2] to recent numerical studies involving DNS. It has hence been shown that the transitional region appears near the trailing edge for low to moderate angles of incidence, and moves towards the leading edge as the angle of incidence increases, and that the bubble length is inversely related to the adverse pressure gradient. More recently, DNS

*Address all correspondence to this author.

simulations performed by Alam et al. (2000) [3] showed that complex and multi-scaled structures can occur in the LSB wake. Pauley et al. (1990) [4] studied an unsteady Laminar Separation Bubble induced by an adverse pressure gradient on a leading edge geometry. They found that the frequency of the vortex shedding from the bubble can be made dimensionless using a Strouhal number $S_{l\theta}$ based on the momentum thickness $(\theta)_{sep}$ and the external velocity $(v_e)_{sep}$ at laminar separation. Moreover, some recent DNS studies showed that those vortex sheddings, resulting from a flapping motion of the bubble, generate characteristic velocity and pressure fluctuations downstream of the bubble, as highlighted by Rist and Maucher (2002) [5] in the case of a flat plate. Recently, Jones et al. (2008) [6] performed a numerical analysis of a LSB in the case of an airfoil at $\alpha = 5^\circ$ and a moderate Reynolds number $Re_c = 5 \times 10^4$. Transition to turbulence was here triggered by a volume forcing, and turbulence development was analyzed in terms of vorticity and wall pressure fluctuations. It appears that the vorticity grows significantly downstream of the LSB location, like in Rist and Maucher (2002) [5] on a flat plate. At the same time, periodic and intermittent pressure fluctuations are found in the near-LSB region, induced by coherent vortex shedding. Far away from the LSB region near the trailing edge, the vorticity increases in a thick boundary-layer and the pressure fluctuations become random, which is characteristic of turbulent fluctuations. Later on, Ducoin et al. (2009) [7] investigated the wall pressure fluctuations along a rigid NACA66 hydrofoil in the case of a transient pitching motion from 0° to 15° . They suggested that the transition together with the vortex shedding of the LSB creates large-amplitude periodic pressure fluctuations downstream of the bubble.

In the case of a flexible foil, such fluctuations are likely to induce important vibrations, that may in return affect the boundary-layer flow. Poirel et al. (2008) [8] have studied the self-sustained oscillations of a NACA0012 airfoil. The low to moderate Reynolds numbers considered suggest that the Laminar Separation Bubble plays an important role in the foil oscillation. Moreover, the laminar to turbulent transition is seen to strongly affect the lift coefficient. Such interactions have also been studied through experimental and numerical approaches for membrane airfoils. Lian et al. (2007) [9], for instance, performed a numerical simulation for $Re = 6 \times 10^4$ of a hydrofoil partly covered with a latex membrane, which was seen to vibrate under the pressure fluctuations generated by the LSB. The presence of this vibrating portion affected the positions of the separation and of the transition, compared to the case of an entirely rigid airfoil in the same conditions, even though the lift and drag mean coefficients are closed to the rigid hydrofoil values. From their numerical simulations involving a latex-membrane airfoil, Visbal et al. (2009) [10] showed that for a low Reynolds number $Re = 2.5 \times 10^3$, the presence

of the fluid lead into a mean camber of the airfoil, as well as large membrane fluctuations for high angles of incidence. The vibrations proved to affect the boundary-layer flow at separation, resulting in improved aerodynamic performances. At a higher Reynolds number $Re = 4.85 \times 10^4$, the boundary-layer was seen to become rapidly turbulent from the leading edge, and the resulting multi-scaled coherent flow structures induce more regular but smaller vibrations.

The aim of the present paper is to investigate, through an experimental study, the vibratory response of flexible a hydrofoil subjected to a transitional regime induced by a Laminar Separation Bubble. Flow velocity and wall pressure measurements are first carried out on a rigid hydrofoil, at given angle of incidence 2° and Reynolds number 0.75×10^6 . The results provide qualitative and quantitative characterizations of the LSB and the following laminar to turbulent transition. A flexible hydrofoil is then considered, and vibration measurements are performed in various configurations, including the same operating conditions as for the rigid hydrofoil. The results are analyzed in light of the previous LSB characteristics, and help to assess the influence of the LSB and transition process on the hydrofoil vibrations.

EXPERIMENTAL SET-UP

Measurements are carried out in the cavitation tunnel at IRE-Nav. The test section is 1 m long and has a square section of length $h = 0.192$ m. The facility provides velocities ranging from 0 to 15 m/s, and pressures from 30 mbar to 3 bars. The tunnel turbulence intensity is about 2%. Both rigid and flexible hydrofoils are NACA 66-shaped, and present a camber type NACA $a = 0.8$, a camber ratio of 2% and a relative thickness of 12% [11]. They are mounted horizontally in the tunnel test section (Figure 1). Their chords $c = 0.150$ m and spans $b = 0.191$ m correspond to a low aspect ratio $b/c = 1.3$ and a confinement parameter $h/c = 1.28$. The hydrofoils can also rotate about an axis located at $x/c = 0.25$. The rigid hydrofoil is made of stainless steel, whereas polyacetate (POM) is chosen for the flexible one.

Pressure measurements are carried out using seventeen piezo-resistive transducers (Keller AG 2 MI PAA100-075-010) of 10 bars maximum pressure. The pressure transducers are mounted into small cavities with a 0.5 mm diameter pinhole at the rigid hydrofoil surface. The wall pressure spectra measured by the transducers are attenuated from the theoretical cut-off frequency $f_c = 9152$ Hz. Experiments are led with a sample frequency of $f = 20$ kHz.

The transducers locations are given in Figure 1. As shown, a set of ten transducers is aligned along the chord on the suction side at mid-span, starting from the leading edge at reduced coordinate $x/c = 0.1$ up to the trailing edge at coordinate $x/c = 0.90$, with a step of $0.10c$. In this paper we will focus on the trans-

ducers located in the LSB region near the trailing edge, that is to say from $x/c = 0.60$ to $x/c = 0.90$. Two sets of three transducers are arranged parallel to this line in order to analyze three-dimensional effects (which are however beyond the scope of this paper).

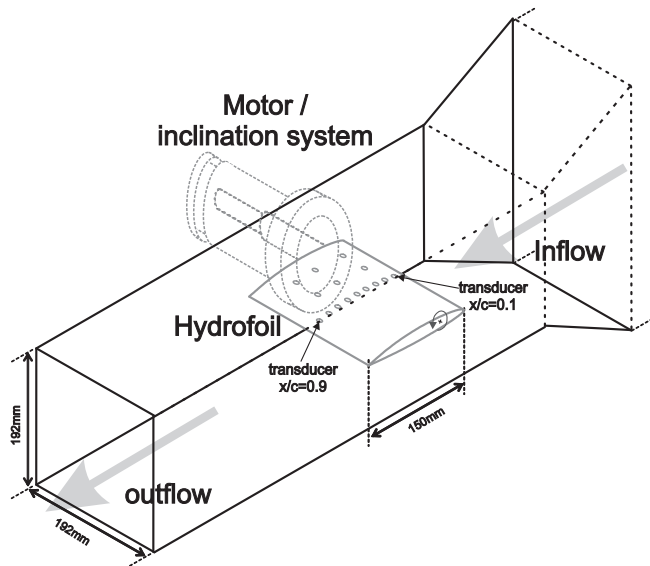


FIGURE 1. Experimental set-up

The nominal free stream velocity V_∞ is 5 m/s, corresponding to a Reynolds number based on the foil chord length of $Re = 0.75 \times 10^6$. The velocities are measured on the suction side of the foil using a DANTEC two component LDA system, providing a 0.5 mm long (Z direction) and 0.04 mm wide (X and Y directions) measuring volume. It was coupled with two DANTEC enhanced Burst Spectrum Analyzers and a DANTEC Burstware software. The origin ($X = 0$, $Y = 0$) of the positioning system is set at the leading edge of the foil at zero angle of incidence. Measurements are performed at $Z = 35$ mm (in the spanwise direction) from the front wall of the test section. The laser beams were aligned with the spanwise direction allowing us to approach closely the surface foil. In our case, only longitudinal velocities u are measured due to the near wall measurements into the boundary layer which is below 1 mm high. Therefore one laser signal is consistently lost. At each measurement location, the resulting velocity corresponds to the time-averaged value over the measurement length. Velocities are mapped along normal lines to the foil surface. The measurement positions along the normals are selected with a logarithmic progression in order to obtain an accurate resolution of the velocity field close to the foil surface, as shown in Figure 2 for $x/c = 0.86$ and $\alpha = 2^\circ$.

The complete measurement grid used during the experiments is summarized in Figure 3. The distribution of the normals

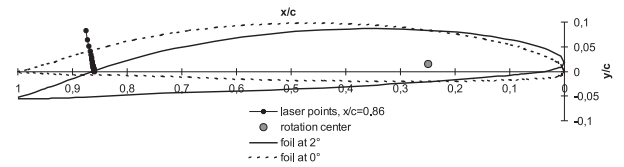


FIGURE 2. LDV measurements along a normal to the hydrofoil surface

along the chord is set according to the knowledge of the LSB location for $\alpha = 2^\circ$, which has been previously studied using wall pressure transducers. Therefore, the mesh is refined near the separation point around $x/c = 0.69$, as well as around the LSB vortex and the turbulent reattachment positions, where transitional boundary layer and high pressure fluctuations occur, that is to say between $x/c = 0.76$ and $x/c = 0.84$. The normal lines are fitted in order to have the first measured point at a $y = 0$ mm coordinate. The random uncertainty associated with the electronic and numerical treatment of the Doppler signal giving the instantaneous velocity is estimated to be less than 1.5%. The uncertainty of the absolute location in the normal direction with respect to the foil surface was of about one tenth of millimeter. Although this error appears small, this implies that a relatively large margin of errors still exists for points in the close vicinity of the foil surface.

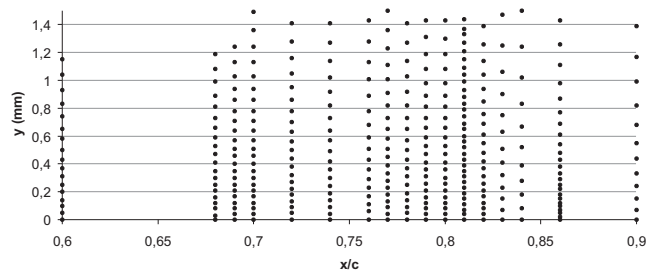


FIGURE 3. LDV measurement grid in the vicinity of the LSB

Structural vibrations are measured by means of a Laser Doppler Vibrometer Polytec PSV-400, using a class II He-Ne laser of wavelength $\lambda = 633$ nm. The device is equipped with a scanning system that enables vibration measurements over a predefined grid mapped on the vibrating surface. The measure is optimized for a plane surface subjected to vibrations in its normal direction, the normal velocities being captured with sensitivities ranging from 10 mm/s/V to 1000 mm/s/V. At each measurement point of the grid, the software provides a Fourier transform of the velocity signal, possibly averaged from a user-defined number of acquisitions, and for frequencies up to 40 kHz. In the following, sets of 32 to 64 acquisitions will be considered to compute

the spectra. Moreover, the preservation of the phase information throughout the scan, thanks to an appropriate reference signal, is useful to retrieve the operating deflection shape at a given frequency, and therefore to identify the natural frequencies of the structure, and their associated vibration modes, from the individual or grid-averaged velocity spectra.

The measurements of the flexible hydrofoil vibrations are performed on the pressure side through the transparent bottom wall of the tunnel test section, the vibrometer scanning head being fixed on the ground. Low-frequency vibrations related to the tunnel structure may hence be detected along with the foil vibrations during the experiment. Considering the geometry of the tunnel test section, the scanning head has to be inclined from its vertical position, the laser beam hence having an angle of incidence with the hydrofoil chord from about 45° near the trailing edge to 90° near the leading edge, as shown in Figure 4.

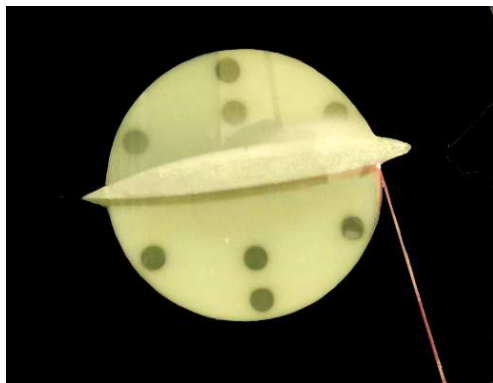


FIGURE 4. Laser vibrometry measurements on the pressure (the straight line is the laser beam)

To improve the accuracy of the results, several single-point vibration measurements have been carried out in addition to scanning measurements over the hydrofoil pressure side. In this configuration, the number of acquisitions used to compute the velocity spectra has been increased, and reflective patches have been stuck on the measurement locations, to avoid the light-absorption effect due to the hydrofoil material.

RESULTS AND DISCUSSION

Velocity measurements

Boundary-layer velocity measurements are carried out for the angle of incidence of 2° around the transitional region. The results are summarized in Figure 5 which shows the velocity profiles along the chord from $x/c = 0.6$ to $x/c = 0.9$. The scenario expected in the case of a transition from laminar to turbulent induced by a LSB is well described. At $x/c = 0.6$, the

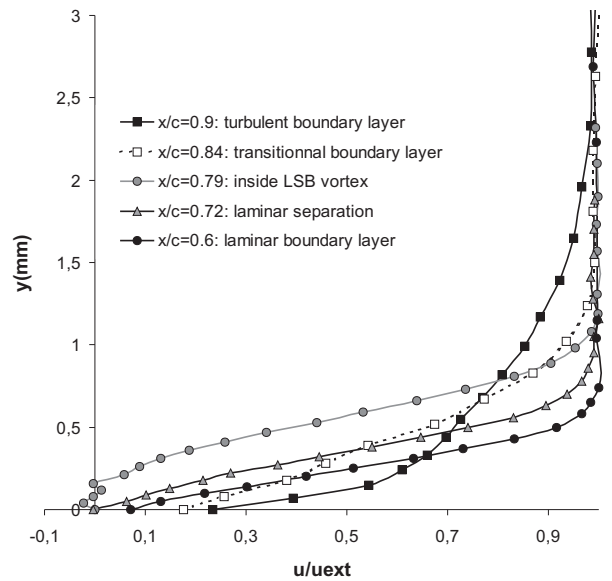


FIGURE 5. Mean velocity profiles from $x/c = 0.6$ to $x/c = 0.9$ for $\alpha = 2^\circ$ and $Re = 750\,000$

boundary layer is thin and laminar. The laminar separation is found at about $x/c = 0.72$, then the velocity profiles are disturbed near the wall, as for instance at $x/c = 0.79$, due to reverse flow. Downstream of this region, a transitional boundary-layer is observed (Figure 5 at $x/c = 0.84$) and the flow is turbulent at about $x/c = 0.9$.

To complete the analysis, the measured values of the longitudinal velocity component u have been gathered and interpolated over the measurement grid (cf. Figure 3). The Figure 6 represents the resulting contour map of the dimensionless velocity u/u_{ext} (with u_{ext} the external velocity to the boundary-layer). The

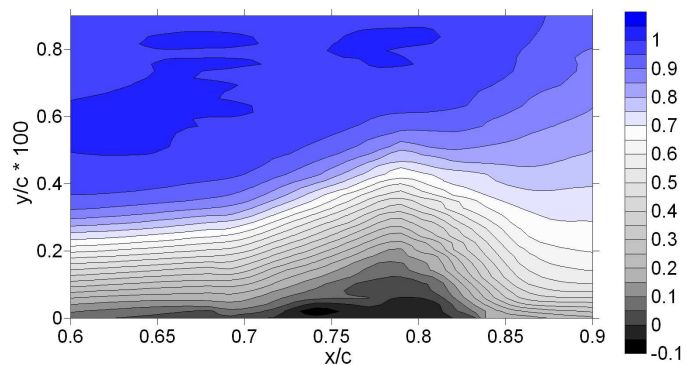


FIGURE 6. Laminar Separation Bubble near the trailing edge: isovalues of the longitudinal velocity component u/u_{ext} through the boundary-layer for $\alpha = 2^\circ$ and $Re = 750\,000$

presence of the LSB, characterized by negative to small positive values, can be easily spotted between $x/c \approx 0.7$ and $x/c \approx 0.82$. The growth of the boundary-layer thickness downstream of the bubble, which reveals the establishment of a turbulent regime, is also clearly visible.

The different stages of the LSB-induced transition are illustrated from the velocity profiles in Figures 7 to 9. The Figure 7 first details the velocity profiles measured between $x/c = 0.6$ and $x/c = 0.74$, which are characteristic of a laminar boundary-layer of thickness less than 1mm. The thinnest boundary-layer is located at $x/c = 0.6$, then the thickness increases as the location gets closer to the trailing edge. Between $x/c = 0.72$ and $x/c = 0.74$, the velocity profiles show an inflection which is identified as the laminar separation.

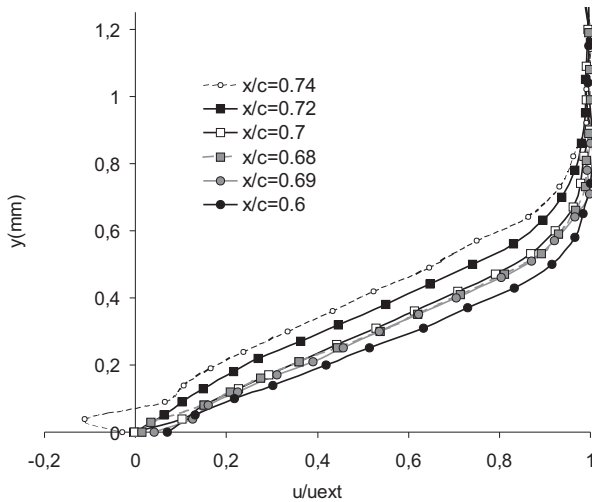


FIGURE 7. Mean velocity profiles at laminar separation ($\alpha = 2^\circ$, $Re = 750000$)

The next velocity profiles, measured between $x/c = 0.76$ and $x/c = 0.81$ into the vortex region of the LSB, are shown in Figure 8. In the close vicinity of the hydrofoil surface, the density of particles needed by the LDV system to estimate the flow velocity decreases which may induce precision errors in the measure of the velocities. In this region, it would hence be hardly feasible to identify the lowest negative and positive velocity components that are expected inside a vortex. Nevertheless, the velocity profiles of Figure 8 clearly exhibit a series of near-zero values close to the surface, which reveal the presence of reversed flow characteristic of the LSB vortex region. Moreover, we observe that the boundary-layer thickness increases up to $x/c = 0.79$ and then decrease up to $x/c = 0.81$. The LSB thickness, which is characterized by a velocity drop in the transition region between the LSB

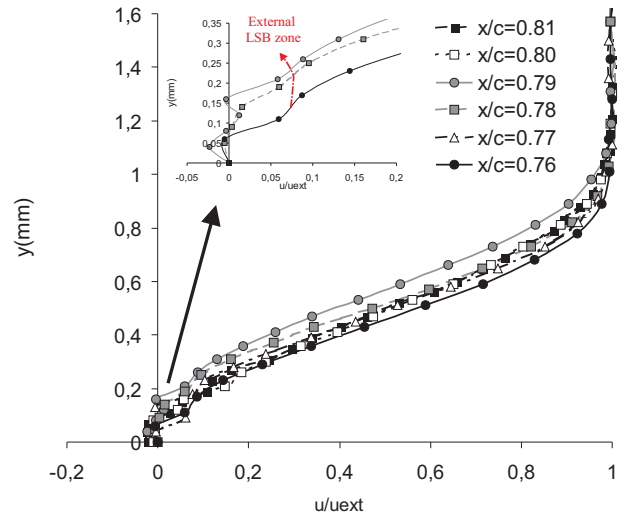


FIGURE 8. Mean velocity profiles in the LSB, vortex region and turbulent reattachment ($\alpha = 2^\circ$, $Re = 750000$)

and the stream flow (see zoom in Figure 8), follows the same evolution. Therefore, the LSB maximum thickness is found for $x/c = 0.79$ and is about 0.2 to 0.25 mm. The turbulent reattachment point of the LSB is located downstream of $x/c = 0.79$, where the velocity profiles show a decrease of the boundary-layer thickness.

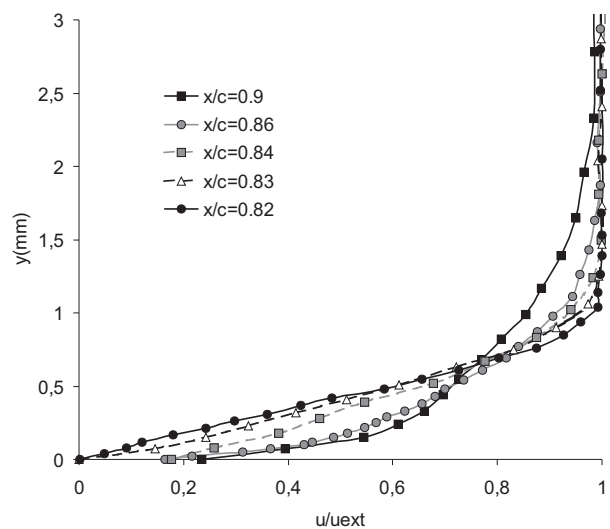


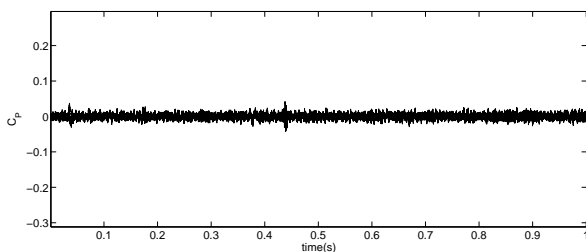
FIGURE 9. Mean velocity profiles around the LSB, transition to turbulence ($\alpha = 2^\circ$, $Re = 750000$)

The Figure 9 illustrates the scenario of transition to turbulence. The boundary-layer is seen transitional from $x/c = 0.82$ to $x/c = 0.84$, with a thickness of about 1 to 1.2mm, and then becomes turbulent from $x/c = 0.86$. The maximum thickness observed on Figure 9 is located at $x/c = 0.9$ and is about 2.2 mm.

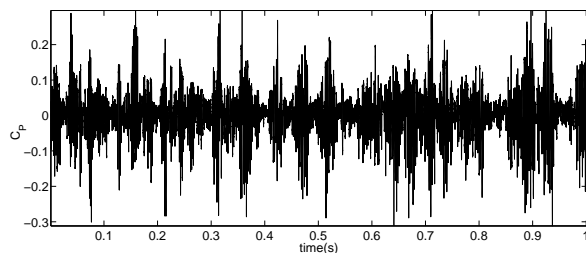
Given the decreasing data rate values at the vicinity of the hydrofoil surface, spectral analyses of velocity fluctuations have not been considered in the present study. However, valuable information can be obtained from spectral analyses of wall pressure measurements, as shown in the next section.

Wall pressure measurements

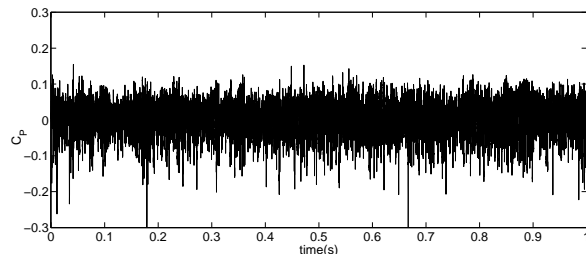
Wall pressure measurements were carried out for $\alpha = 2^\circ$ during a period of $T = 1$ s. The results are shown in Figure 10 for three locations $x/c = 0.7$, $x/c = 0.8$ and $x/c = 0.9$. No fluctuations are visible at $x/c = 0.7$, Figure 10 (a). Assuming that the laminar separation is located between $x/c = 0.72$ and $x/c = 0.74$,



(a) $x/c = 0.7$



(b) $x/c = 0.8$

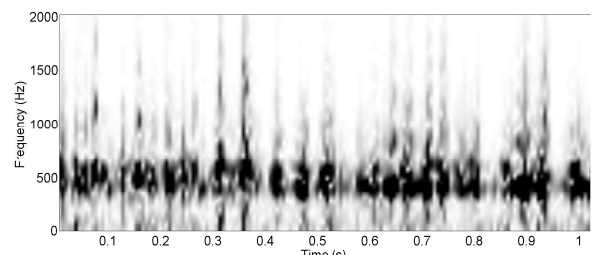


(c) $x/c = 0.9$

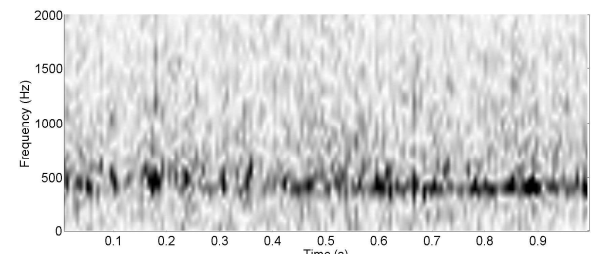
FIGURE 10. Wall pressure fluctuations for a static angle of incidence $\alpha = 2^\circ$ and various transducers along the suction side, $Re = 750000$

the pressure transducer therefore lays in the laminar and unperturbed boundary-layer. At $x/c = 0.8$ (Figure 10 (b)), high amplitude fluctuations of about $\Delta C_p = 0.3$ are observed, characterized by an intermittent behavior. Moreover, these fluctuations seem periodic and are located around the turbulent reattachment of the LSB (see Figure 8), where the boundary-layer is highly disturbed. Then, at $x/c = 0.9$ (Figure 10 (c)), the level of fluctuations decreases ($\Delta C_p \approx 0.1$) and gets denser within an approximately constant envelope, confirming the turbulent behaviour of the boundary-layer at this location.

The pressure signal fluctuations are post-processed using spectrograms to highlight possible characteristic frequencies. The spectrograms are short-time frequency spectra computed from signal segments of 256 points, that is, considering the sampling frequency $f = 20$ kHz, of length $T = 0.0128$ s. For each time-segment, a Fast Fourier Transform is computed using a Hamming window, with a precision $\Delta f = 4.88$ Hz. An overlap of 50% (that is, 128 points) is chosen between the segments, and the frequency spectra are hence estimated every 0.0064 s. The spectrograms of the two fluctuating pressure signals, corresponding to $x/c = 0.8$ and $x/c = 0.9$, are depicted in Figure 11. For $x/c = 0.8$ (Figure 11 (a)), the spectrogram presents high-amplitude frequency peaks, relatively localized between a main frequency $f \approx 400$ Hz, and a secondary frequency about 600 Hz. These fluctuations are clearly not turbulent, but the consequence of a vortex shedding process with an intermittent behavior. Downstream of this location, the fluctuations appear to be more random, as a result of the turbulence development (Figure



(a) $x/c = 0.8$



(b) $x/c = 0.9$

FIGURE 11. Spectrograms of wall pressure fluctuations at $\alpha = 2^\circ$ for two transducers along the suction side, $Re = 750000$

11 (b)). It may be noticed that the main frequency of the vortex shedding $f \approx 400$ Hz is still visible, however with a lower amplitude.

Further Fourier transform computations of the wall pressure fluctuations have been performed to get a more precise value of the specific frequencies mentioned above. For this purpose, two sets of Fast Fourier Transforms are computed for the later transducer locations $x/c = 0.8$ and $x/c = 0.9$, using pressure signals recorded over a period of length $T = 4$ s with a timestep $\Delta T = 5.10^{-4}$ s. The precision of the Fourier transforms is therefore $\Delta f = 0.25$ Hz. The resulting average frequency spectra for the two locations are shown in Figure 12. The trends raised from the analysis of the previous spectrograms are retrieved, and the dominating vortex shedding frequency may be estimated as $f = 395$ Hz, whereas the secondary frequency is about 576 Hz.

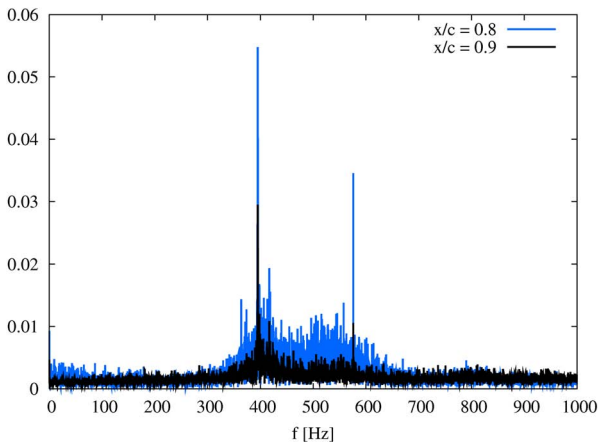


FIGURE 12. Frequency spectra of the wall pressure fluctuations at $x/c = 0.8$ and $x/c = 0.9$ for $\alpha = 2^\circ$ and $Re = 750000$

At higher angles of incidence $\alpha \geq 5^\circ$, it was observed that the transition is located at the leading edge of the hydrofoil, and the boundary-layer is fully turbulent over the whole suction side. Examples of spectrograms, obtained for $\alpha = 6^\circ$ at the same locations $x/c = 0.8$ and $x/c = 0.9$ as previously, are shown in Figure 13. Both spectra exhibit a large range of random frequencies associated to low amplitudes, without any dominating peak as for the previous turbulent spectrum for $\alpha = 2^\circ$. These spectrograms hence confirm the presence of a fully turbulent boundary-layer flow that does not result from a LSB process.

LSB characteristics

Table 1 details the boundary-layer characteristics along the suction side of the hydrofoil for $\alpha = 2^\circ$, deduced from the velocity measurements.

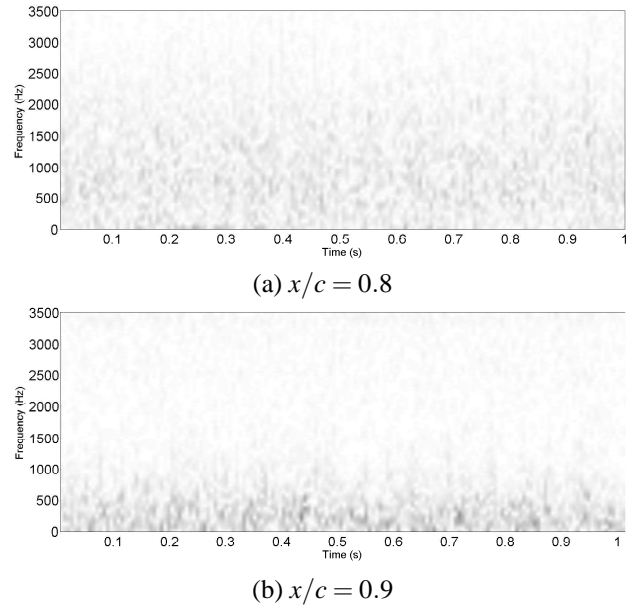


FIGURE 13. Spectrograms of wall pressure fluctuations at $\alpha = 6^\circ$ for two transducers along the suction side, $Re = 750000$

The boundary-layer is characterized by the shape coefficient defined as $H = \frac{\delta^*}{\theta}$, with δ^* the boundary-layer displacement thickness and θ the boundary-layer momentum thickness. This parameter is useful to localize the laminar separation, where H reaches a value of 3.5, and discriminate the laminar boundary-layer, for which $H = 2.6$, from the turbulent one, characterized by $H = 1.6$ (according to previous numerical studies). First, the results obtained at $x/c = 0.6$, where $H = 2.43$, meets the expected value for a laminar boundary-layer. The laminar separation may then be located between $x/c = 0.72$ and $x/c = 0.74$, where H ranges between 3.379 and 3.959. The LSB region is then observed between $x/c = 0.76$ and $x/c = 0.81$ and is characterized by H values larger than 3.5. At $x/c = 0.83$, the shape factor reaches the value of $H \approx 2$ characteristic of a transitional boundary-layer, and then a turbulent value $H = 1.61$ is retrieved at $x/c = 0.86$.

From the boundary-layer characteristics, it is possible to compute the Strouhal number $S_{t\theta}$ of the LSB vortex shedding, defined from the vortex shedding frequency f , the momentum thickness at separation $(\theta)_{sep}$ and the external velocity at separation $(u_{ext})_{sep}$, as $S_{t\theta} = \frac{f \times (\theta)_{sep}}{(u_{ext})_{sep}}$. For a laminar separation occurring at $x/c = 0.72$, using the frequency $f = 395$ Hz and the velocity $(u_{ext})_{sep} \approx 5.8$ m/s determined through LDV measurements, we obtain a Strouhal number $S_{t\theta} = 0.0076$, which is close to the value of $S_{t\theta} = 0.0068$ found in Pauley et al. (1990) [4]. To take into account the uncertainty in the determination of the separation location, a mean Strouhal number may be computed from

the average momentum thickness and external velocity between $x/c = 0.68$ and $x/c = 0.74$, which gives the value even closer of $S_{r\theta} = 0.0074$. This confirms that the periodic pressure fluctuations observed in our experiments result from a vortex shedding process downstream of a Laminar Separation Bubble.

TABLE 1. Boundary-layer characteristics for $\alpha = 2^\circ$ and $Re = 750000$

Location on chord	$\delta^*(\text{mm})$	$\theta(\text{mm})$	H
0.6	0.230	0.095	2.43
0.68	0.317	0.104	3.049
0.69	0.307	0.108	2.852
0.7	0.338	0.108	3.119
0.72	0.379	0.112	3.379
0.74	0.447	0.113	3.959
0.76	0.499	0.123	4.050
0.77	0.534	0.127	4.198
0.78	0.564	0.124	4.548
0.79	0.544	0.124	4.383
0.8	0.466	0.128	3.619
0.81	0.529	0.132	4.025
0.82	0.472	0.171	2.757
0.83	0.382	0.167	2.286
0.84	0.395	0.185	2.139
0.86	0.403	0.250	1.61
0.9	0.457	0.287	1.593

Vibration measurements

Vibration measurements have been carried out on the flexible hydrofoil for various angles of incidence and freestream velocities. In the following, results of single-point measurements on a reflective patch located near the trailing edge are presented, along with scanning measurements over the whole pressure side of the hydrofoil. For the latter, a grid of 9×9 measurement points in the longitudinal and spanwise directions and a frequency bandwidth of $[0; 2]$ kHz have been chosen in order to recover an accurate description of the first modes of the hydrofoil. The visualization of the operating deflection shapes at the resonance frequencies observed on the vibration spectra enables the mode identification, as shown in Figure 14 for the modes 2 to 4. The first four natural frequencies of the hydrofoil have hence been determined as $f_1 = 43$ Hz (first bending mode), $f_2 = 171$ Hz (first torsional

mode), $f_3 = 291$ Hz (second bending mode) and $f_4 = 560$ Hz (mixed bending and torsional mode).

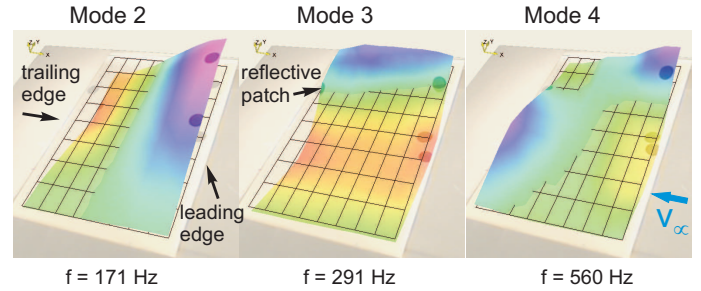


FIGURE 14. Experimental mode shapes obtained from scanning measurements at the grid points

Figure 15 compares the spectra of the normal displacement velocity of the hydrofoil measured on the reflective patch (observable in Figure 14) for the free stream velocity $V_\infty = 5$ m/s and three angles of incidence $\alpha = 2^\circ$, $\alpha = 4^\circ$ and $\alpha = 6^\circ$. Considering first the two extreme values, the corresponding spectra both exhibit resonance peaks at the first natural frequencies of the hydrofoil, but additional peaks appear around 450 Hz for $\alpha = 2^\circ$. As discussed in the previous sections, such frequencies may be related to the vortex shedding process induced by the LSB that exists at this low angle of incidence. This is confirmed by the fact that no additional contributions are visible on the spectrum obtained at $\alpha = 6^\circ$, for which the boundary-layer is fully attached and turbulent all over the hydrofoil surface.

The vortex shedding frequency was estimated about 400 Hz from the analysis of pressure spectrograms (Figure 11). Considering the values of the additional components observed on the velocity spectra, it seems that the frequencies associated with the vortex shedding process are slightly increased in the presence of the flexible hydrofoil, which may be due to the fluid-structure interaction between the hydrofoil and the boundary-layer. The LSB vortex shedding may be affected by the vibrations at the fourth natural frequency, which are particularly enhanced, as compared to the fully turbulent case, by the shedding excitation at close frequencies. The presence of the laminar to turbulent transition also explains the increase of vibration levels between the two spectra. However, the present measurements do not allow us to raise conclusions regarding the influence of the hydrofoil flexibility on the transition.

Vibration measurements have been performed at intermediate angles of incidence, for which the boundary-layer is subjected to laminar separation before becoming turbulent. The velocity spectrum obtained for instance for $\alpha = 4^\circ$, at the same Reynolds number $Re = 750000$, is very similar to the previous

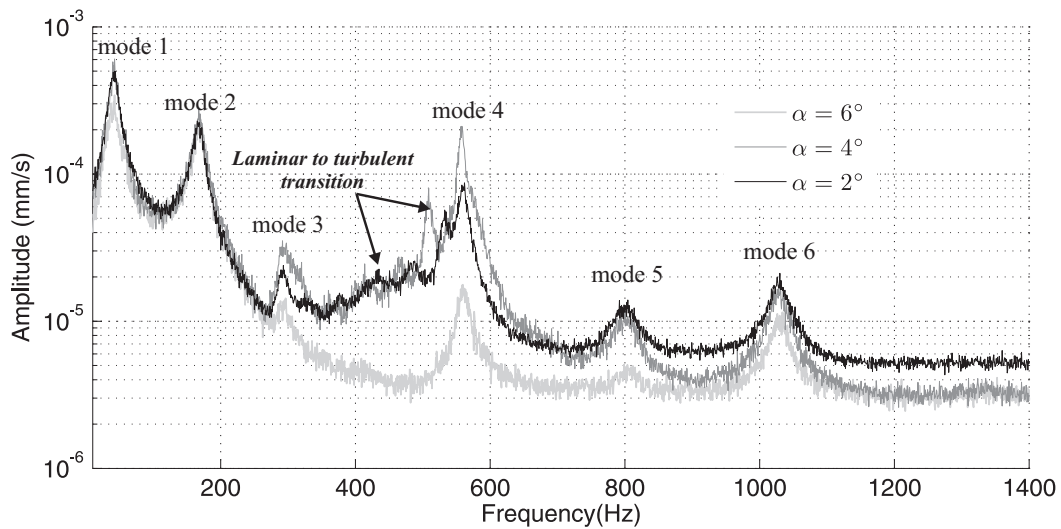


FIGURE 15. Hydrofoil normal velocity spectra for $\alpha = 2^\circ$, $\alpha = 4^\circ$ and $\alpha = 6^\circ$, $Re = 750000$

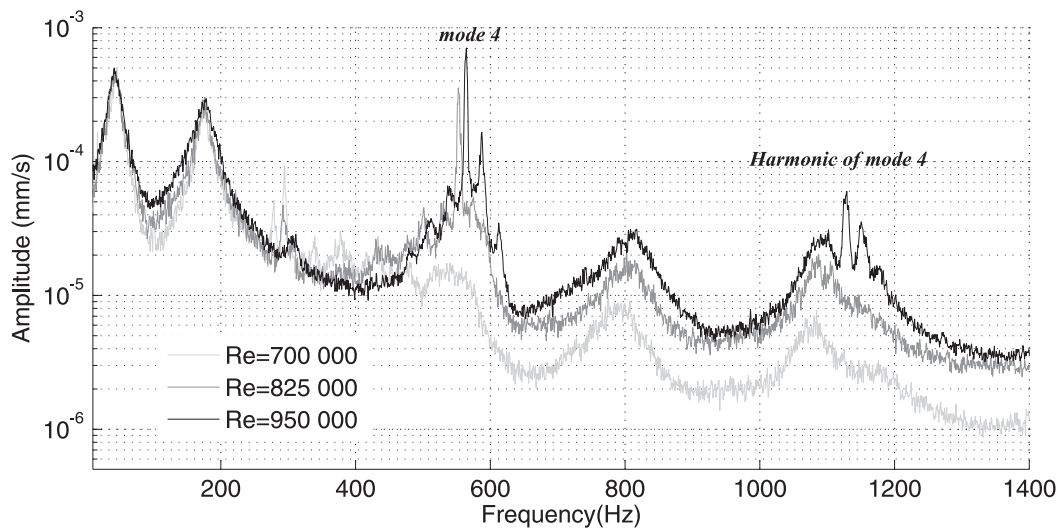


FIGURE 16. Comparison of hydrofoil velocity spectra for $\alpha = 4^\circ$ and various Reynolds numbers

one for $\alpha = 2^\circ$, showing only slight amplitude variations around the fourth natural frequency (see Figure 15). This observation is consistent with the fact that although the LSB comes closer to the leading edge as the angle of incidence increases, the boundary-layer thickness is very little modified in this region, hence the LSB keeps overall the same characteristics (see Ducoin et al. (2009) [7]).

Additional measurements, carried out at various Reynolds numbers and angles of incidence, have shown that a variation of the free stream velocity could have on the contrary a strong

impact on the LSB and the induced hydrofoil vibrations. Examples of hydrofoil velocity spectra computed from the vibration measurements at $\alpha = 4^\circ$ and three Reynolds numbers are displayed in Figure 16. It appears that the amplitude of the additional components related to the LSB vortex shedding process increases with the Reynolds number, inducing a coherent growth of the surrounding modal peaks (apart from the first two modal peaks which remain similar whatever the Reynolds number). As reported for instance in Pauley et al. (1990) [4], the frequencies introduced by the vortex shedding and the transition are also seen to increase with the Reynolds number, and the interaction

with the modal vibrations varies accordingly. For the smallest Reynolds number considered in our experiments, $Re = 700\,000$, the LSB-induced frequency hence seems close to the third natural frequency of the hydrofoil, resulting in an enlargement of the corresponding peak in the vibration spectrum. For the larger value $Re = 950\,000$, the amplification of the fourth modal peak reveals that the shedding frequency has now increased towards the fourth natural frequency. For the latter case, the amplitudes of the modal peak and the surrounding additional components are such that harmonics are visible in the higher frequency domain, resulting again in a more complex interaction with the upper-ranked modes.

CONCLUSION

In this paper, we have presented a characterization of the Laminar Separation Bubble that may be observed in the boundary-layer along a hydrofoil, together with an analysis of the hydrofoil vibrations induced by the LSB, through an experimental study. Flow velocity measurements have been used to determine, for given freestream velocity and angle of incidence, the localization and the size of the LSB on a rigid hydrofoil. Laminar to turbulent transition and turbulent reattachment have also been explored. A vortex shedding process induced by the LSB has been identified from the observation of periodic structures in wall-pressure fluctuations measurements along the rigid hydrofoil. The vortex shedding frequency has been computed from a post-processing. We have then studied the behaviour of a flexible hydrofoil in the same operating conditions. The vortex shedding and the transition process are seen to enhance the vibrations of the hydrofoil, especially at frequencies close to that of the vortex shedding. We observe that depending on their natural frequencies, some vibration modes are therefore likely to interact strongly with the boundary-layer flow along the hydrofoil. Further experiments are needed to assess the influence of the hydrofoil vibrations on the LSB and the transition process.

REFERENCES

- [1] Gaster, M., 1969. *The structure and behaviour of laminar separation bubbles*, ARC R&M 3595. HMSO.
- [2] Tani, I., 1964. "Low-speed flows involving bubble separations". *Progress in Aerospace Sciences*, **5**, pp. 70–103.
- [3] Alam, M., and Sandham, N. D., 2000. "Direct numerical simulation of short laminar separation bubbles with turbulent reattachment". *Journal of Fluid Mechanics*, **410**, pp. 1–28.
- [4] Pauley, L. L., Moin, P., and Reynolds, W. C., 1990. "The structure of two-dimensional separation". *Journal of Fluid Mechanics*, **220**, pp. 397–411.
- [5] Rist, U., and Maucher, U., 2002. "Investigations of time-

- growing instabilities in laminar separation bubbles". *European Journal of Mechanics/B Fluids*, **21**(5), pp. 495–509.
- [6] Jones, L. E., Sandberg, R. D., and Sandham, N. D., 2008. "Direct numerical simulations of forced and unforced separation bubbles on an airfoil at incidence". *Journal of Fluid Mechanics*, **602**, p. 175.
- [7] Ducoin, A., Astolfi, J., Deniset, F., and Sigrist, J., 2009. "Computational and experimental investigation of flow over a transient pitching hydrofoil". *European Journal of Mechanics/B Fluids*, **28**, pp. 728–743.
- [8] Poirrel, D., Harris, Y., and Benaissa, A., 2008. "Self-sustained aeroelastic oscillations of a NACA0012 airfoil at low-to-moderate Reynolds numbers". *Journal of Fluids and Structures*, **24**(5), pp. 700–719.
- [9] Lian, Y., and Shyy, W., 2007. "Laminar-turbulent transition of a low Reynolds number rigid or flexible airfoil". *AIAA Journal*, **45**(7), pp. 1501–1513.
- [10] Visbal, M. R., Gordnier, R. E., and Galbraith, M. C., 2009. "High-fidelity simulations of moving and flexible airfoils at low Reynolds numbers.". *Experiments in Fluids*, **46**, pp. 903–922.
- [11] Leroux, J. B., Coutier-Delgosha, O., and Astolfi, J. A., 2005. "A joint experimental and numerical study of mechanisms associated to instability of partial cavitation on two-dimensional hydrofoil". *Physics of Fluids*, **17**, p. 052101.